Analysis of Material-Related Instability Problems for Inelastic Thin Shells

Takaya Kobayashi and Yasuko Mihara

Mechanical Design & Analysis Corporation

Abstract*: The buckling of axially compressed cylindrical shells is known to be sensitive to imperfections, as is the buckling of spherical shells under external pressure. Regarding these problems, a very slight imperfection can be the starting point from which local deformation is initiated and developed and, consequently, overall structural stability is lost. Therefore, it has been very difficult to pursue an analysis using the conventional approach, which is typically represented by the arc-length method. The methodology developed in our previous study demonstrates the applicability of the artificial damping method of Abaqus from which we can overcome the difficulty in performing the analysis due to local instability. This paper describes the application of the technique for the generation of singularities in large-deformed viscoelastic and elastoplastic cylindrical shells, which is expected to be utilized in the packaging of food, daily articles, and pharmaceuticals.*

Keywords*: Shell, Buckling, Riks method, Artificial damping, Viscoelasticity*

1. Introduction

Geometrically nonlinear static problems sometimes involve buckling or collapse behavior, in which the load-displacement response shows a negative stiffness and the structure must release strain energy to remain in equilibrium. Several approaches can be used to model such behavior. Among them, path tracing, based on the arc-length method, is the most fundamental procedure. This method is used for cases in which the loading is proportional, that is, in which the load magnitudes are governed by a single scalar parameter. If the analysis process traces unstable paths under the global load-displacement response with negative stiffness, the arc-length method is effectively usable. However, if the instability is localized (e.g., surface wrinkling, material instability, or local buckling), there will be a local transfer of strain energy from one part of the model to the neighboring parts, and global solution methods may not work. This class of problems must be solved either dynamically or with the aid of artificial damping. The buckling of a real, thin-walled shell is typically a local phenomenon, and it may be triggered by a small, local disturbance. In terms of the buckling problem related to elastic cylindrical shells under axial compression, experimental results have shown that after primary buckling, secondary buckling occurs, accompanied by successive reductions in the number of circumferential waves at every path jumping. In a previous study, the authors traced this successive buckling of the elastic cylindrical shells using the latest general-purpose finite element technology with a static artificial damping method (Kobayashi, 2012). The study accomplished a fully automatic and seamless simulation of successive path jumpings in the deep post-buckling region and showed good agreement with Yamaki's experimental results (1984) and Esslinger's high-speed photography (1970). This paper describes the examples of the application of the artificial damping technique: the generation of singularities in large-deformed viscoelastic cylindrical shells under axial compression, as well as wrinkling during elastoplastic cup drawing.

2. Artificial damping method

The artificial damping method is a technique used to achieve total energy balance in static analysis, compensating for strain energy changes due to local elastic instability. In the present study, Abaqus (Dassault, 2013), the general-purpose finite element code, was used due to its powerful nonlinear capability to overcome the analytical instabilities encountered in thin-shell problems, while the artificial damping method or its comparable quasistatic capabilities are available in other codes, such as ADINA, ANSYS, and Marc. Abaqus provides an automatic mechanism for stabilizing unstable quasi-static problems through the automatic addition of volume-proportional damping to the model. Via Equation (1), viscous forces are added to the global equilibrium equations, as shown in Equation (2):

$$\mathbf{F}_{\mathrm{v}} = c\mathbf{M}^{*}\mathbf{v} \tag{1}$$

$$\mathbf{P} - \mathbf{Q} - \mathbf{F}_{\mathrm{v}} = \mathbf{0} \tag{2}$$

where $\mathbf{M}^{*}$ is an artificial mass matrix calculated with unity density, c is a damping factor, $\mathbf{v} = \Delta\mathbf{u}/\Delta t$ is the vector of nodal velocity, $\Delta\mathbf{u}$ is the vector of incremental displacement, Δt is the increment of time (which may or may not have a physical meaning in the context of the problem being solved), $\mathbf{P}$ is the total applied load, and $\mathbf{Q}$ is the internal force. When local instability occurs, the deformation rate of that portion begins to increase, and locally released strain energy is dissipated due to the appended damping effect. Consequently, quasi-static analysis makes it possible to treat the problems involved in local instability.

Empirically, as is the case in general, moderate stabilizing can be achieved by adjusting the damping factor c in Equation (1) so that the total dissipated energy does not exceed 1–10% of the total strain energy. In terms of Abaqus use, the damping factor c is specified by an indirect input parameter called "the dissipated energy fraction," which is the ratio of the allowable incremental damping energy (the dissipated energy for a given increment) to the total strain energy. The fraction has a default value of 2.E-4. The damping factor for each individual element is adjusted to meet the requirements at both the global and the local element level. However, since the artificial damping energy is classified as non-conservative, the resultant energy always increases, while the strain energy may decrease. Therefore, the above-mentioned treatment is just a target and can be corrected in some situations, such as when there is rigid body motion or when significant non-local instability occurs. In such cases, the damping factor is chosen such that the average element damping matrix component, divided by the step time, is equal to the average element stiffness matrix component multiplied by the dissipated energy fraction.

Based on our practical experience, lowering the dissipated energy fraction to 1/100–1/1,000 of the default value (2.E-4) provides highly sensitive analytical performance (Kobayashi, 2012). This technique is useful, for instance, to achieve precise expressions of the mode jumping along with the sharp dropping of the load for thin shell problems.

3. Viscoelastic cylindrical shells under axial compression

The time-dependency of the material properties can affect the buckling behavior. Taking the viscoelasticity of resin materials as an example, this kind of material-related instability may occur in the formation process of thin-walled structures, such as the blow-forming of plastic containers or the formation of polymer thin films. In this study, we performed experimental and analytical investigations of viscoelastic cylindrical shells under axial compression. The generation of singularities was studied in comparison with the elastic cylindrical shells.

For The test shells were constructed from Mylar (polyethylene terephthalate) film. Because the Mylar film has both a high elastic limit and also a glass transition temperature lower than 100 °C, the buckling experiment can be easily conducted in the glass transition temperature region of the material. Figure 1 shows the storage modulus E', the loss modulus E'', and the loss tangent tanδ as functions of temperature. These dynamic viscoelastic properties of the Mylar film were measured for angular velocities 3.16, 10, 31.6, and 100 rad/sec with an ascending temperature rate of 2 °C/min in the temperature range of 30 to 200 °C. A TA Instruments RSA III dynamic mechanical analyzer was used to measure the dynamic viscoelastic properties. This measurement device is equipped with a temperature-controlled oven with a solid structure and a high volume flow rate, providing excellent performance in temperature control. The glass transition temperature T_g was estimated to be 70 °C. To create a master curve, the WLF formula, as shown below, was applied for the time-temperature reduction.

$$\log\big(\alpha(T)\big) = -\frac{C_1(T-T_{\mathrm{R}})}{C_2+(T-T_R)} \qquad (3)$$

where

$$T_{\mathrm{R}} = T_{\mathrm{g}} + 50,\ \ T_{\mathrm{g}} = 70\ ℃,\ \ C_1 = 8.86,\ \ C_2 = 101.6$$

The generalized Maxwell model is the most general form of the linear model of viscoelasticity. It takes into account that the relaxation does not occur at a single time but at a distribution of times. The coefficients for the generalized Maxwell model were obtained from the master curve via the optimization approach so that the relaxation curve from Equation (4) could be calculated numerically. The relationship between time-domain constants and frequency-domain constants is expressed as shown in Equation (5) and Equation (6). Using these formula, the numerical constants for the generalized Maxwell model (Equation (4)), which provides a close approximation of the actual measurement data, can be obtained.

$$E_{\mathrm{r}}(t') = E_{\mathrm{e}} + \sum_{n-1}^{N} E_{\mathrm{n}} \exp(-t'/\tau_n) \qquad (4)$$

$$E' = E_{\mathrm{e}} + \sum_{n=1}^{N} \frac{\tau_{\mathrm{n}}^2 \omega'^2}{1+\tau_{\mathrm{n}}^2 \omega'^2} E_{\mathrm{n}} \quad (5)$$

$$E'' = \sum_{n=1}^{N} \frac{\tau_{\mathrm{n}} \omega'}{1+\tau_{\mathrm{n}}^2 \omega'^2} E_{\mathrm{n}} \quad (6)$$

where

E_{r}: relaxation modulus,
E_{e}: long-term modulus once the material is totally relaxed,
E_{n}: elastic modulus of the n^{th} Maxwell element,
τ_{n}: relaxation time of the n^{th} Maxwell element,
N: number of Maxwell elements in parallel.

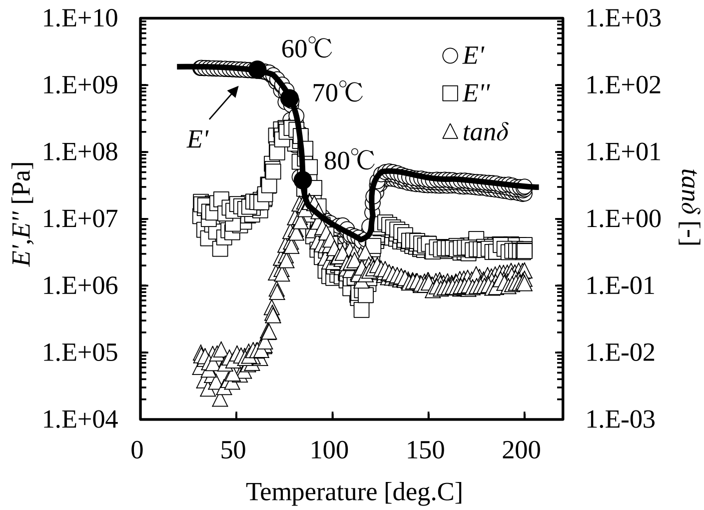

Figure 1. Dynamic viscoelastic properties for Mylar film.

Material Buckling test temperatures of 60, 70 (= T_{g}), and 80 °C were assigned so that each temperature corresponded to the glassy condition, the glass transition condition, or the rubbery condition, respectively. Figure 2(a) to Figure 2(c) show the relaxation curves for each temperature. According to the time–temperature superposition principle, the curves, as a function of time, do not change shape as the temperature is changed but appear to only shift left or right based on Equation (5). With the planned time duration of the buckling test set at 300 sec, the estimated relaxation zones (1–300 sec) are indicated in the figures. As is clear from the figures, the zones are located across the glassy condition, the glass transition condition, or the rubbery condition.

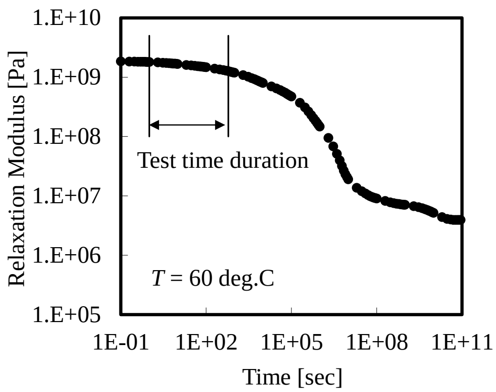

(a) 60 °C; Glassy condition

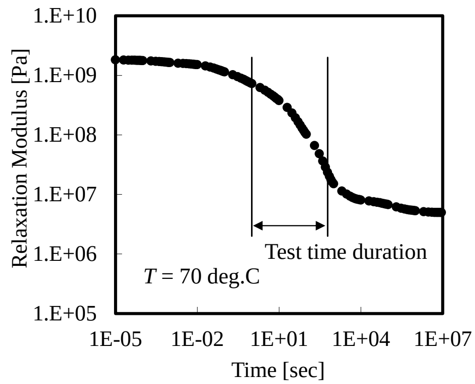

(b) 70 °C; Glass transition condition

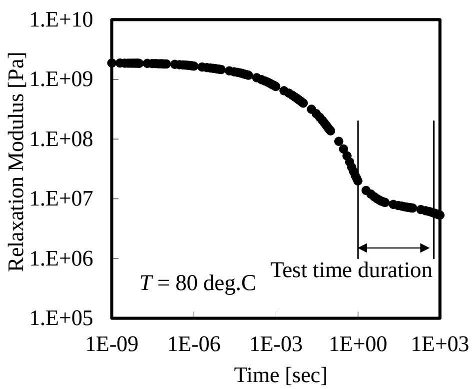

(c) 80 °C; Rubbery condition

Figure 2. Relaxation curves for Mylar film.

We have confirmed that the uniaxial FE model provides results that are identical to the experimental data shown in Figure 2. The viscoelastic property of the Mylar film, especially its temperature dependency, was precisely measured so that it could serve as the background for achieving this agreement (Kobayashi, 2012-2). Figure 3 shows the compression test results for the cylindrical shells under each test temperature. The test shells, with a diameter of 80 mm, a height of 100 mm, and a wall thickness of 0.30 mm, were created with a simple longitudinal lap joint. The shells were fully fixed at both ends into a thick aluminum plate and were compressed at a constant temperature bath up to an axial shortening of 5 mm in 300 sec. The test temperatures were 60, 70, and 80 °C, as mentioned above. The buckling behaviors varied depending on these temperature conditions.

Figure 4 shows the load-shortening curves. The analytical results showed close agreement with the experimental results. In the glassy condition (60 °C), the test shell showed typical elastic buckling behavior accompanied by successive reductions in the number of circumferential waves (from n = 8 to n = 6) at every path jumping. Likewise, the test shell buckled with an elastic deformation of n = 8 within the glass transition region (70 °C). However, in this case, the strain energy was relieved immediately due to stress relaxation, and consequently, the initial buckling pattern remained as a permanent deformation as shown in Figure 3(b). In the rubbery condition (80 °C), although the elastic buckling still provided the specific deformation mode of n = 8 in the very early stage of the buckling process, the initial buckling shape was replaced immediately by an irregularly deformed shape with a round edge due to rapid stress relaxation as shown in Figure 3(c).

(a) 60 °C; Glassy condition

(b) 70 °C; Glass transition condition

(c) 80 °C; Rubbery condition

Figure 3. Viscoelastic buckling of Mylar cylindrical shells under axial compression: Experiment (left); FEM (right).

In general, a change in elastic modulus due to viscoelastic relaxation has a range of ten to the third power or more, as shown in Figure 2. Viscoelastic material properties actually provide stabilizing effects regarding dynamic aspects. However, in a static scheme, the rapid decrease in elastic modulus may cause the loss of structural stability. The artificial damping method also overcomes analytical difficulties due to material-related instability because the instantaneous stiffness change can be reflected in the global equilibrium equations with appropriately adjusting the damping force so as to correspond to the states of the local and individual instabilities in the model. Incidentally, the explicit dynamic method is poorly suited to lengthy events (empirically more than one second).

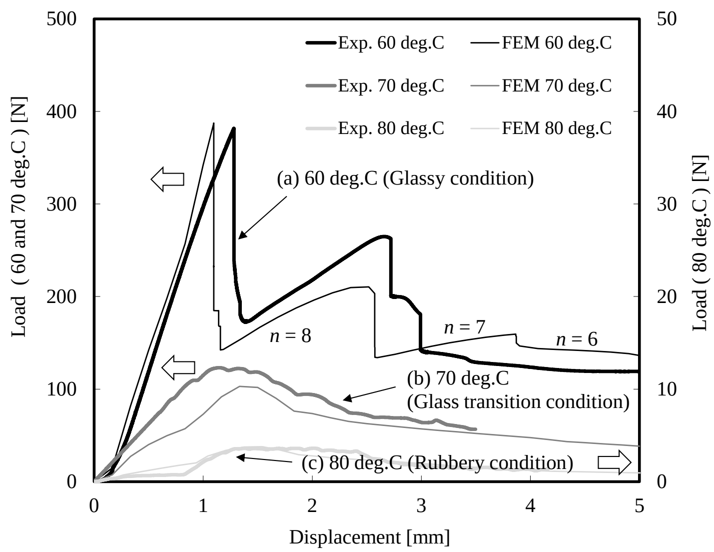

Figure 4. Load-shortening curves for each temperature condition.

4. Wrinkling during elastoplastic cup drawing

This problem is presented as a benchmark at the 9th International Conference and Workshop on Numerical Simulation of 3D Sheet Metal Forming Processes (NUMISHEET 2014) (Dick, 2014). Advanced can manufacturing technology and cost control efforts have resulted in a consistent reduction of the net metal weight used, which has led to beverage cans with thinner sidewalls, reduced neck diameters, and smaller base diameters. However, small-diameter cans increase the likelihood of wrinkling during production, as show in Figure 5. A schematic view of tools used for the drawing process, including their dimensions, is shown in Figure 6. The drawing occurs continuously during one punch stroke, and the punch speed is 140 mm/sec. The recommended friction coefficient is 0.03, and the blank holding force is given as 8900 N. AA 5042 aluminum alloy (t = 0.2083mm) and aluminum-killed draw-quality (AKDQ) steel (t = 0.2235mm) are considered as sheet materials. These materials are assumed to have the YLD2000 anisotropic yield criteria (Barlat, 2003), as shown in Figure 7, in which s_{11} and s_{22} represent the stress in the rolling direction and the stress in the transverse direction, respectively. The anisotropic elasto-plastic material behaviors were implemented in Abaqus by using the UMAT user-defined material subroutine.

Experiment FEM

Figure 5. Draw cup with wrinkles.

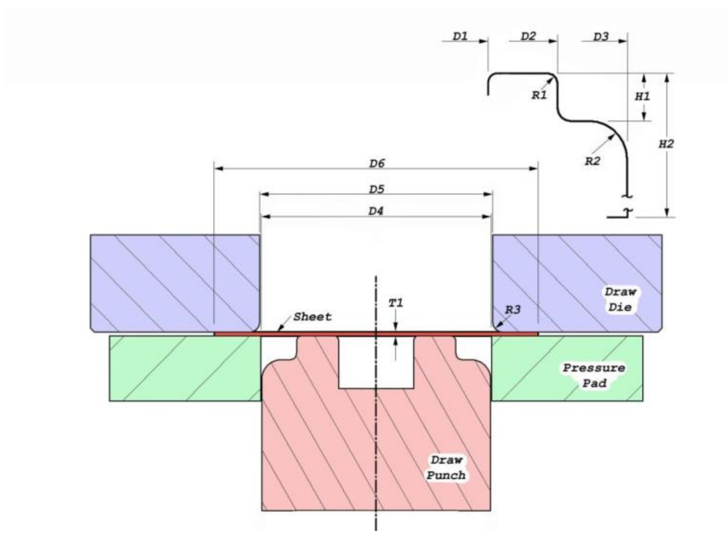

Figure 6. Schematic view of tools for the drawing process (Dick 2014).

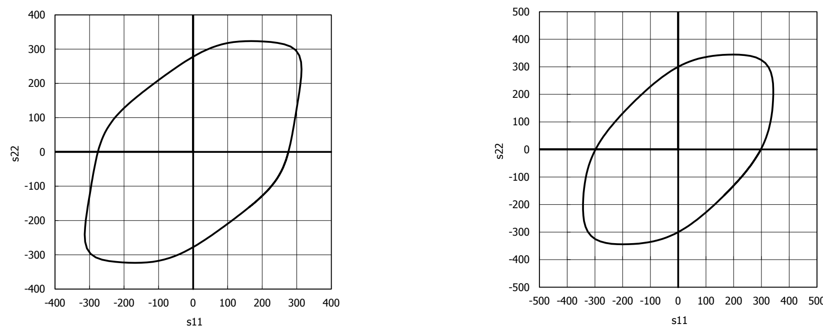

(a) AA5042 aluminum alloy (b) AKDQ steel

Figure 7. Anisotropic yield surfaces.

In this study, we traced the local buckling behavior of anisotropic elasto-plastic thin shells using the artificial damping method. The automatic seamless simulation provided good agreement with the experimentally observed buckling behavior, which covered the entire drawing process well, as shown in Figure 8. While explicit dynamic codes have been conventionally used in the field of sheet metal forming analysis, one of the practical advantages of using implicit codes is that they make it possible to calculate eigenmodes at any midpoint in the analysis. Figure 9(a) shows the results from the eigenvalue analysis for AA5042. The eigenvalue analysis was performed at a very early stage of the punching process (2 mm of stroke). The magnitude of this punch stroke is small enough that one can assume a nearly uniform circumferential stress distribution on the shell. The plastic strain generated at this point was around 1–2%. One noteworthy fact is that all the extracted eigenvalues were negative. This means that the buckling is triggered by a relaxation of the punching stress of the sheet, which may be due to the development of the plastic strain of the sheet and/or the sheet sliding out from the draw die.

The curves in Figure 9(a) represent the relationship between the normalized eigenvalue λ and the number of circumferential full-waves n, where m is the number of radial half-waves. In the vicinity of the lowest critical value, multiple eigenmodes with different numbers of waves (n = 7–12 for m = 1) exist. The proximity of the eigenmodes must have impaired the reproducibility of the experiments; our history analysis of the punching process (Figure 8(a)) provides a unique buckling mode with n = 12. On the other hand, the curves for AKDQ do not indicate any obvious minimum point, as shown in Figure 9(b). This suggests that the deformation of the sheet tends to remain axisymmetric (n = 0) and that the punching process does not show local buckling behavior. Our history analysis for AKDQ (Figure 8(b)) supports this estimation.

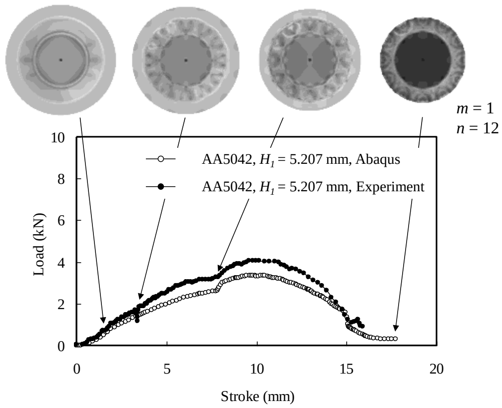

(a) AA5042 aluminum alloy

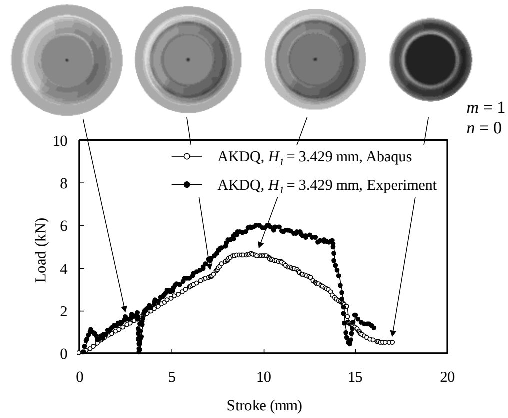

(b) AKDQ steel

Figure 8. Load-stroke diagram during the drawing process.

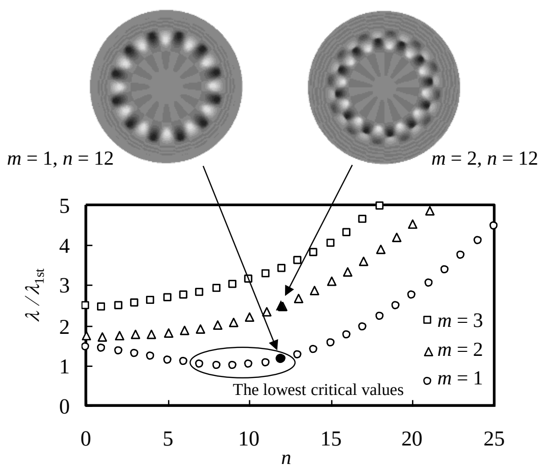

(a) AA5042 aluminum alloy

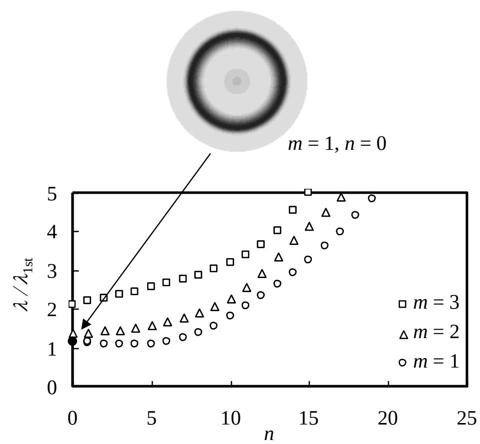

(b) AKDQ steel

Figure 9. A Relationship between the normalized eigenvalue and the number of circumferential full-waves *n*.

The buckled area on the shell can be regarded as a circular plate with a hole at the center and the inner and outer boundaries clamped. Timoshenko (1961) suggested that such a circular plate, when subjected to radial loading, buckles in multiple waves along the circumference. When the ratio of the inner and outer radii approaches unity, the buckling conditions for a compressed ring are analogous to those of a long, compressed rectangular plate. In the case of the rectangular plate, a typical deformation mode indicates several half-waves in the direction of compression but only one half-wave in the perpendicular direction, as shown in Figure 10. The lengths of the half-waves are supposed to approach the width of the plate because a buckled plate is subdivided approximately into squares. A single eigenvalue will be extracted for this deformation mode.

However, manufacturing experience indicates that the real process conditions, such as the mechanical properties of the metal sheet, the tooling geometry, and the contact conditions (including lubrication), cause multiple buckling modes with different numbers of circumferential waves in close proximity. This suggests that the effective width of the buckled area is influenced by the above-mentioned factors. In fact, the conference organizer reported that the number of circumferential full-waves was found to be n = 13 (AA5042) and n = 11 (AKDQ) in their benchmark experiment, whereas our analyses provides n = 12 (AA5042) and n = 0 (AKDQ). The relationship between the eigenmodes obtained from the linear eigenvalue analysis and the deformation modes actually observed in the buckling process requires further investigation.

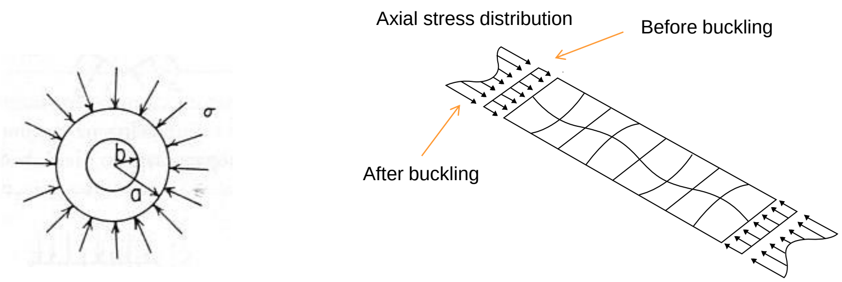

Figure 10. Analogy of buckling behavior between a compressed ring (left) and compressed rectangular plate (right).

5. Conclusion

In designing a modern lightweight structure, it is of technical importance to ensure its safety against buckling under the applied loading conditions. This study presents the application of the artificial damping method to practical material-related instability problems. Replacing the kinetic energy with the artificial damping energy makes it possible to analyze instability problems within the static analysis scheme. The proposed technique is useful not only for elastic local buckling problems but also for material-related instability problems.

6. References

1. Abaqus Users Manual, Dassault Systems Simulia Corp., 2013, Version 6.13, USA.
2. Barlat, F., Brem, J.C., Yoon, J.W., Chung, K., Dick, R.E., Lege, D.J., Pourboghrat, F., Choi, S.H. and Chu, E., 2003, Plane stress yield function for aluminum alloy sheets—part 1: theory, International Journal of Plasticity, 19, 1297–1319.
3. Dick, R., Cardoso, R., Yoon, J.W. and Paulino, M., 2014, Benchmark 4, The 9th International Conference and Workshop on Numerical Simulation of 3D Sheet Metal Forming Processes (NUMISHEET2014), Melbourne, http://www.numisheet2014.org/
4. Esslinger, M., 1970, Hochgeschwindigkeitsaufnahmen von Beulvorgang dunnwandiger, axialbelasteter Zylinder, Der Stahlbau, 39 (3), 73-76.
5. Kobayashi, T., Mihara, Y. and Fujii, F., 2012, Path-Tracing Analysis for Post-buckling Process of Elastic Cylindrical Shells under Axial Compression, Thin-Walled Structures, 61, 180–187.
6. Kobayashi, T., Sato, M. and Mihara Y., 2012, Application of Thermo-Viscoelastic Laminated Plate Theory to Predict Warpage of Printed Circuit Boards, Viscoelasticity, Juan de Vicente (Editor), InTech, ISBN 980-953-307-335-9.
7. Timoshenko, S.T. and Gere, J.M., 1961, Theory of Elastic Stability, 2nd ed., McGraw-Hill, New York, pp.389–392.
8. Yamaki, N., 1984, Elastic Stability of Circular Cylindrical Shells, North-Holland, Netherlands, p.222.